Cellulose (2024) 31:1397–1415
https://doi.org/10.1007/s10570-023-05702-x

ORIGINAL RESEARCH

Matrix polysaccharides affect preferred orientation of cellulose crystals in primary cell walls

Sintu Rongpipi · William J. Barnes · Oskar Siemianowski · Dan Ye · Joshua T. Del Mundo · Sydney Duncombe · Xiaoran Xin · Chenhui Zhu · Michael F. Toney · Ying Gu · Charles T. Anderson · Enrique D. Gomez · Esther W. Gomez

Received: 17 June 2023 / Accepted: 14 December 2023 / Published online: 9 January 2024

Abstract The spatial organization and interactions of constituent components influence cell growth and determine physical and chemical properties of the cell wall, including its rigidity, flexibility, and degradability. Elucidating the interactions between cell wall polysaccharides is crucial for advancing our knowledge of how cell walls are assembled and for designing approaches to efficiently break down cell walls to produce renewable energy and biomaterials. Here, we investigated the effect of defects in the biosynthesis of cell wall components on the nanoscale organization of cellulose in primary cell walls through grazing incidence wide angle X-ray scattering (GIWAXS) measurements of hypocotyls of wild type *Arabidopsis thaliana* and of cellulose, pectin, and xyloglucan (hemicellulose) deficient mutants. GIWAXS reveals changes in lattice spacings, coherence lengths, and relative crystalline content for cellulose between wild type and mutant plants. In addition, X-ray pole figures constructed using GIWAXS and X-ray diffraction (XRD) rocking scans quantify an emerging measure of cellulose organization, the degree of preferred orientation (texture) of cellulose crystals with respect to the cell wall plane. Comparing X-ray pole figures from pectin-deficient and xyloglucan-deficient mutants to that of wild type plants reveals that cellulose texture is disrupted in pectin-deficient mutants,

Supplementary Information The online version contains supplementary material available at https://doi.org/10.1007/s10570-023-05702-x.

S. Rongpipi · D. Ye · J. T. Del Mundo · E. D. Gomez (✉) · E. W. Gomez (✉)
Department of Chemical Engineering, The Pennsylvania State University, University Park, PA 16802, USA
e-mail: edg12@psu.edu

E. W. Gomez
e-mail: ewg10@psu.edu

W. J. Barnes · O. Siemianowski · S. Duncombe · C. T. Anderson
Department of Biology, The Pennsylvania State University, University Park, PA 16802, USA

X. Xin · Y. Gu
Department of Biochemistry and Molecular Biology, The Pennsylvania State University, University Park, PA 16802, USA

C. Zhu
Advanced Light Source, Lawrence Berkeley National Laboratory, 1 Cyclotron Road, Berkeley, CA 94720, USA

M. F. Toney
University of Colorado Boulder, Boulder, CO 80309, USA

E. D. Gomez
Department of Materials Science and Engineering and Materials Research Institute, The Pennsylvania State University, University Park, PA 16802, USA

E. W. Gomez
Department of Biomedical Engineering, The Pennsylvania State University, University Park, PA 16802, USA

but not in xyloglucan mutants. Our results indicate that a deficiency of pectin during cell wall biosynthesis alters cellulose organization in plant cell walls.

Keywords Grazing-incidence wide-angle X-ray scattering · Rocking scan · Crystal texture · *Arabidopsis thaliana* · Pole figure · Relative crystalline cellulose content

Introduction

Cellulose microfibrils are synthesized by a multiprotein, rosette-like cellulose synthase complex (CSC), which contains six globular units that each consist of multiple cellulose synthase (CESA) catalytic subunits (Cosgrove 2005; Lerouxel et al. 2006; Taylor 2008). CSCs move within the plasma membrane while depositing crystalline microfibrils into an amorphous wall matrix composed of hemicellulose and pectins. The spatial organization of cell wall components and interactions between them impact the development, growth, and mechanical properties of plants (Preston 1974; Carpita and Gibeaut 1993; Xiao et al. 2016; Zeng et al. 2017; Rongpipi et al. 2019).

Defects in the biosynthesis of cell wall components likely alter the structure and properties of the cell wall. Indeed, altered cellulose structure and organization have been found in primary (growing) cell walls of cellulose deficient mutants that lack fully functional CESA or CSC-associated genes (Gu et al. 2010; Harris et al. 2012; Lei et al. 2014; Turner and Kumar 2018). For example, reduced cellulose crystallinity has been seen in mutants with defects in CESA3 and CESA6 proteins (Fagard et al. 2000; Rui and Anderson 2016) and in CSC-associated non-CESA proteins, such as CELLULOSE SYNTHASE INTERACTIVE PROTEIN 1 (CSI1) (Gu et al. 2010) and KORRIGAN 1 (KOR1) (Takahashi et al. 2009; Lei et al. 2014). The cellulose coherence length (often taken as crystal size) and crystallinity decrease in *Arabidopsis thaliana* plants with mutations in the C-terminal transmembrane domain region of CESAs, including CESA1^{A903V} and CESA3^{T942I} (Harris et al. 2012). Studies have also reported reduced crystalline cellulose content, altered CSC activity, and altered mesoscale organization of cellulose microfibrils in pectin deficient *qua2-1* and *tsd2-1* mutants and in the xyloglucan deficient *xxt1 xxt2* mutant of *Arabidopsis thaliana* (Cavalier et al. 2008; Xiao et al. 2016; Du et al. 2020). Macroscale changes in cellulose organization, such as bundling of cellulose microfibrils into macrofibrils, has been shown in petal epidermal cell walls with decreased level of pectin rhamnogalaturonan-I (Saffer et al. 2023). Xyloglucan deficient *xxt1 xxt2* mutants also exhibit macroscale changes in cell walls, such as uneven and rippled cell walls (Yu et al. 2022).

While previous work has examined the effects of altered biosynthesis of cell wall components on the mesoscale organization of cellulose in primary cell walls (MacKinnon et al. 2006; Xiao et al. 2016; Du et al. 2020), details regarding the nanoscale organization of cellulose, such as cellulose crystal plane spacing, coherence length, and crystallite orientation with respect to the cell wall plane, remain underexplored. These nanoscale structural parameters for cellulose can be important determinants of cell growth and mechanics (Zhang et al. 2021). Insights into the effects of wall composition on these parameters can help elucidate relationships between nanoscale structure and macroscale properties of primary cell walls in plants.

Grazing-incidence wide-angle X-ray scattering (GIWAXS) is a powerful technique to examine the structure and orientation of crystals within various materials, including organic semiconductors and polymeric coatings (Rivnay et al. 2012; Hexemer and Müller-Buschbaum 2015). Recently, GIWAXS was applied for the study of plant cell walls, where the grazing-incidence geometry revealed diffraction from cellulose crystals oriented along and perpendicular to the cell wall plane, and thereby provides a measure of the preferred orientation of cellulose crystals along the thickness of primary cell walls of onion epidermis, Arabidopsis hypocotyls, and moss phyllids (leaves) (Ye et al. 2020). The degree of preferred orientation of cellulose crystals, or crystal texture, is apparent from χ-pole figures constructed using the combination of GIWAXS and X-ray rocking scans, and the integrated intensity of these χ-pole figures is proportional to the crystal content (χ is the polar angle in GIWAXS 2D data).

Here, GIWAXS reveals the nanoscale organization of cellulose in hypocotyls of wild type and mutants of 6-day-old dark-grown seedlings of *Arabidopsis thaliana*. We compare the lattice parameters, crystal coherence lengths, preferred orientations of crystals

along the cell wall thickness, and relative crystalline content of cellulose between wild type seedlings and mutants with defective cellulose, pectin, and xyloglucan. Our experiments reveal that the preferred orientation of cellulose crystals is disrupted in pectin and cellulose mutants, but not in xyloglucan mutants. Cellulose also has a higher degree of disorder in cellulose deficient mutants than in wild type samples, as evidenced by larger lattice spacing (more loosely packed chains) and smaller crystal coherence lengths. The relative crystalline cellulose content of hypocotyls is also lower in cell wall mutants than in wild type plants. In addition, we track a recently identified measure of cellulose organization (Ye et al. 2020; Del Mundo et al. 2023), the degree of preferred orientation of cellulose crystals with respect to the cell wall plane, and find that it correlates with hypocotyl length. Altogether, our GIWAXS data suggest that defective biosynthesis of cellulose and non-cellulosic wall components alters normal cellulose organization, and in particular, altered pectin in the wall matrix likely disrupts the organization of cellulose crystals in primary plant cell walls.

Materials and methods

Plant materials and growth conditions

Arabidopsis hypocotyls

The *Arabidopsis thaliana* Columbia (Col-0) ecotype was used as the wild type in this study. In addition, the cellulose deficient mutants *cesa3*^{je5}*(je5)* (Desprez et al. 2007), *cesa6*$^{prc1-1}$*(prc1-1)* (Desnos et al. 1996), *csi1-3* (Gu et al. 2010), and *jia1-1*(Lei et al. 2014); pectin deficient mutants *qua2-1* (Mouille et al. 2007) and *tsd2-1* (Krupková et al. 2007); xyloglucan deficient mutant *xxt1 xxt2* (Xiao et al. 2016), and the *TmXXT2/xxt1 xxt2* complementation line (Mansoori et al. 2015) were used to examine the impact of cellulose, pectin, and xyloglucans on cell wall structure. Seeds were sterilized in 30% bleach solution containing 0.1% (w/v) sodium dodecyl sulfate (SDS) for 20 min with occasional mixing, washed in sterile water four times, resuspended in 0.15% agar (Sigma), and stored at 4 °C for 2–7 days for vernalization. Seeds were sown on ½ Murashige and Skoog (MS) plates wrapped in two layers of aluminum foil to induce etiolation and grown in a 22 °C chamber for 6 days before harvesting, flash-freezing, and storage at − 80 °C until sample preparation. The ½ MS medium contained 2.2 g/L MS salts (Caisson Laboratories), 0.6 g/L 2-N-morpholino-ethanesulfonic acid (MES; Research Organics), and 0.8% (w/v) agar–agar (Research Organics) at pH 5.6.

The T-DNA insertional mutant of *csi1-3* (SALK_138584) was obtained from the Arabidopsis Biological Resource Center (ABRC). The *jia1-1* mutant was previously characterized and published (Lei et al. 2014). Seeds of *csi1-3* and *jia1-1* mutants were surface sterilized with 30% (v/v) bleach for 15 min, thoroughly washed with sterile double-distilled water (ddH_2O) and stored at 4 °C for a minimum of 3 days. Seedlings were grown on vertical ½ MS plates without sucrose for 6 days at 21 °C in the dark.

GIWAXS and rocking scan sample preparation

Hypocotyls of 6-day-old dark grown *Arabidopsis thaliana* seedlings were washed in 0.1% Tween-20 in 20 mM HEPES buffer (pH 6.8) for 1 h with shaking at 50 rpm and then washed with deionized (DI) water to remove debris.

Silicon substrates for GIWAXS experiments were cleaned by sonication in acetone, iso-propanol, and DI water, sequentially. Organic impurities were removed from the silicon surfaces by ultraviolet (UV)/ozone cleaning. For GIWAXS and rocking scan measurements, 30 hydrated hypocotyls, each approximately 15 mm long, were mounted flat, side-by-side on a silicon substrate and then air dried. Hypocotyls were macroscopically flat once dried.

GIWAXS data collection and analysis

GIWAXS experiments were performed at beamline 7.3.3 of the Advanced Light Source (ALS) at Lawrence Berkeley National Laboratory (Hexemer et al. 2010) and beamline 11–3 of Stanford Synchrotron Radiation Lightsource (SSRL) at the SLAC National Accelerator Laboratory. Samples mounted on silicon substrates were examined in a helium environment to minimize background scattering. Data were collected at the ALS using 10 keV X-rays and a Pilatus detector with an incident angle of 0.15°. Data were collected at SSRL using 12.7 keV X-rays and a Rayonics 225

detector with an incident angle of 0.12°. For analysis, GIWAXS 2D images were corrected for the curvature of the Ewald sphere using Xi-cam (Pandolfi et al. 2018) for data collected at ALS and using WxDiff (Mannsfeld 2010) for data collected at SSRL. Scattering data are expressed as a function of the scattering vector $q = \frac{4\pi\sin(\theta)}{\lambda}$ where θ is half the scattering angle and λ is the wavelength of the incident X-ray. q_{xy} and q_z are the parallel and perpendicular components of the scattering vector with respect to the substrate, respectively. The out-of-plane scattering profile was obtained by integrating over polar angles (χ) from − 17° to + 17° (where 0° is along the vertical direction), and the in-plane scattering profile was obtained by integrating data with polar angles between + 78° and + 88°. Three or more independent samples were measured for each condition to ensure repeatability.

Rocking scan data collection

Rocking scans were carried out at Experimental Station 11–3 of SSRL at the SLAC National Accelerator Laboratory. Data were collected using 12.7 keV X-rays and a Rayonics 225 detector. Rocking scans for the cellulose (1 $\bar{1}$ 0)/(110) reflection were measured in the specular set-up by rocking the samples at $4.4° \le \theta \le 5.9°$ corresponding to 0.99 $Å^{-1} \le q \le 1.31$ $Å^{-1}$. Three or more independent samples were measured for each condition to ensure repeatability.

Background subtraction

Background correction for χ-pole figures was performed as previously reported (Ye et al. 2020). A local background was subtracted from the azimuthal integration of the cellulose (1 $\bar{1}$ 0)/(110) reflection in both GIWAXS and rocking scan data. An azimuthal integration along polar angle (χ) of a region outside the (1 $\bar{1}$ 0)/(110) reflection was selected as the local background. The azimuthal sector with a q-range from 0.6 to 0.7 $Å^{-1}$ was selected as local background for GIWAXS data. The intensity of the local background at each polar angle was subtracted from the intensities of azimuthal cuts over the (1 $\bar{1}$ 0)/(110) reflection at the corresponding polar angle. Similarly, the region corresponding to a q-range of 1.8 $Å^{-1}$ to 1.9 $Å^{-1}$ was selected as background for rocking scans. The integrated intensities of these regions were subtracted from the intensities of the azimuthal cuts over the (1 $\bar{1}$ 0)/(110) reflection in rocking scan data at the corresponding polar angle.

Pole figures

A pole figure represents the distribution of orientation of crystallographic planes, and we denote χ-pole figures as representing the orientation with respect to the substrate surface. χ-pole figures for the cellulose (1 $\bar{1}$ 0)/(110) reflection were constructed as previously reported (Ye et al. 2020). Partial pole figures with polar angles (χ) between − 90° to − 7.5° and 7.5° to 90° were obtained by azimuthally integrating the (1 $\bar{1}$ 0)/(110) reflection over $q = 1.15 \pm 0.16$ $Å^{-1}$ from corrected GIWAXS images. Data for pole figures near the specular direction were obtained from rocking scans. A sector integration was performed for the (1 $\bar{1}$ 0)/(110) reflection at $q = 1.15 \pm 0.16$ $Å^{-1}$ within $-30° < \chi < 30°$ of the 2D rocking scan images. To construct the complete χ-pole figure, a scaling factor was used to scale the background corrected GIWAXS data to match rocking scan data at $\chi = \pm 7.5°$ as previously reported (Ye et al. 2020).

Degree of preferred orientation and relative crystalline cellulose content

The degree of preferred orientation or texture of crystallites can be quantified from the widths (full width at half maximum, FWHM) of χ-pole figures (Widjonarko et al. 2014). The degree of preferred orientation of cellulose crystals was determined from the width of χ-pole figures of the cellulose (1 $\bar{1}$ 0)/(110) reflection, which were corrected for the background as described above. The width of the pole figure is inversely related to the degree of preferred orientation (i.e., a narrower pole figure corresponds to a higher degree of preferred orientation). The widths of pole figures were determined from the FWHM obtained by fitting to a Lorentzian function.

The relative crystalline cellulose content can be obtained from integrating the intensity (I) over polar angle from $\chi = -90°$ to 90° of χ-pole figures corrected by sine of χ to account for the decrease in observed intensity with increasing χ resulting from the fiber or 2D crystallographic texture (random

orientation of crystallites in the substrate plane) (Jimison 2011; Rivnay et al. 2012):

$$\text{Relative crystalline cellulose content} \propto \int_0^{\pi/2} I(\chi)\sin(\chi)d\chi.$$

The relative crystalline cellulose content of Arabidopsis hypocotyls is calculated from sin(χ) corrected χ-pole figures at the cellulose (1 $\bar{1}$ 0)/(110) reflection. Under the assumption that the relative crystalline cellulose content is independent of the sample thickness, the integrated intensity is linearly related to the sample thickness (Widjonarko et al. 2014). The integrated intensity is normalized by the sample thickness obtained from stylus profilometry to account for the effects of thickness on the intensity of pole figures. The sample size along the beam direction was maintained the same (within a few percent) to ensure intensities can be compared between samples.

Crystal d-spacing and crystal coherence length

Cellulose crystal d-spacing and crystal coherence length were estimated from out-of-plane scattering intensity profiles obtained by integrating the scattering intensity over polar angles from − 17° to + 17°. Varying the polar angle range from 15° to 20° does not affect scattering profiles or peak positions of cellulose reflections (Fig. S1). The crystal coherence length is often taken to be equivalent to the crystal size, although this ignores paracrystallinity and other defects (Zhang et al. 2019). The crystal d-spacing (d) of the cellulose (1 $\bar{1}$ 0)/(110) and (200) planes was calculated from the values of the scattering vector, q, at which the reflections occur in the out-of-plane scattering profile through $d = 2\pi/q$. Cellulose crystal coherence length (τ) was estimated from line broadening of the cellulose (200) reflection in the GIWAXS out-of-plane intensity profile through Scherrer's equation (Patterson 1939):

$$\tau = \frac{k\lambda}{\beta\cos\theta}$$

where λ is the X-ray wavelength, θ is the Bragg angle, k is a shape factor that we take as 0.89, and β is the angular FWHM of the line profile. To obtain peak positions and line broadening of cellulose reflections, a linear background obtained from $q \sim 0.05$ Å^{-1} to 2.0 Å^{-1} was subtracted from GIWAXS out-of-plane intensity profiles. The background subtracted GIWAXS out-of-plane intensity profiles were deconvoluted to obtain the cellulose (1 $\bar{1}$ 0), (110), and (200) reflections using Lorentzian functions.

Stylus profilometry

Sample thickness was measured using a Tencor P16 Stylus profilometer. Each GIWAXS sample was scanned at 9 different locations along the length of the hypocotyls. Thicknesses were estimated from averages of 27 measurements from three samples of each genotype.

Cell length measurements

Plant material

Arabidopsis thaliana (Col-0 ecotype) seeds expressing Low Temperature Induced Protein 6B-green fluorescent protein (LTI6b-GFP), a plasma-membrane marker (Cutler et al. 2000), were grown as previously described. Then 6-day-old seedlings were used to measure cell lengths.

Measurements

The hypocotyl cell lengths were measured using confocal images obtained using a Zeiss Axio Observer SD microscope with a Yokogawa CSU-X1 spinning disk head and a 10× air objective with a 0.3 numerical aperture. GFP was detected using a 488-nm excitation laser and a 525/50-nm emission filter. The consecutive slightly overlapping pictures were stitched and analyzed in ImageJ (Rueden et al. 2017) using the following protocol: (i) the scale was set based on confocal image metadata (pixel size), (ii) the images were made semi-transparent to obtain the best match of cell wall pattern during overlaying (without resizing to keep a constant scale), (iii) the transparency effect was removed from the images of whole continuous stitched hypocotyls and each cell was outlined based on GFP signal (expression of LTI6b-GFP plasma-membrane marker) using the polygon tool while keeping the geometry as close to rectangular as possible, (iv) the height of each polygon was used to calculate the cell length, and (v) the mean cell length

was calculated for 3 zones of hypocotyls defined as: top (0–1 mm from cotyledon), bottom (0–1 mm from root), and middle (region 2 mm below cotyledon and 2 mm above root). The cell length of the middle region was calculated by averaging cell lengths in the region below 2 mm from cotyledon and 2 mm above root. Statistical differences were assessed based on a single factor ANOVA Q test, with $p < 0.05$.

Updegraff measurements

Crystalline cellulose content was measured in 6-day-old etiolated (dark grown) Arabidopsis seedlings using the Updegraff method (Updegraff 1969). Seedlings were incubated in 80% ethanol at 65 °C overnight. After removal of ethanol, the seedlings were incubated with acetone overnight at room temperature and were then allowed to dry in a fume hood. The air-dried residue was ball milled for 3 min at room temperature using a Retsch Cryomill. After weighing the resulting powder, the powder was suspended in a solution of acetic acid:nitric acid:water at a ratio of 8:1:2 at 100 °C for 30 min. Pellets were sedimented for 5 min at 20,000 g and resuspended in 67% sulfuric acid (Sigma). Absorbance at OD_{620} was read for samples in 1 mL of 0.2% anthrone (w/v; Sigma) in concentrated sulfuric acid using a spectrophotometer (NanoDrop 2000C). D-Glc (Sigma) was used as a standard for calculation of cellulose content in samples.

Hypocotyl length measurements

The lengths of *Arabidopsis* hypocotyls of Col-0, cesa3^{je5}, *cesa6*$^{prc1-1}$, *csi1-3, jia1-1,* and *TmXXT2/xxt1 xxt2* ecotypes/genotypes were measured using ImageJ software after 6 days of growth. The mean hypocotyl length was calculated for at least n = 35 seedlings for each genotype.

Statistical analyses

All experimental results are from at least three biological replicates. The data are represented as the mean ± standard error of the mean. Statistical analyses were performed using a Student's t-test or ANOVA to evaluate whether differences were significant in comparison to the wild type sample. In addition, 95% confidence intervals of the differences of means were also calculated to examine whether the confidence interval contains the null hypothesis value (Altman and Krzywinski 2017).

Results

GIWAXS reveals structure of crystalline cellulose in plant cell walls

Grazing incidence wide angle X-ray scattering (GIWAXS) relies on a small incident angle, near the critical angle for X-rays, to reveal diffraction from crystalline structures with enhanced signal-to-noise when compared to transmission or specular reflection geometries. Figure 1a shows GIWAXS data taken with a 2D detector for 6-day-old dark grown hypocotyls of the wild type *Columbia* (Col-0) ecotype of *Arabidopsis thaliana*. Scattering along the plane of the cell wall is visible along the horizon, whereas out-of-plane scattering is visible along the meridian. GIWAXS can reveal a preferred orientation of crystals by examining the intensity as a function of polar angle. Previous work showed that anisotropic Bragg reflections seen in GIWAXS 2D data of primary cell walls of onion epidermal peels, Arabidopsis hypocotyls, and moss leaves at $q = 1.15$ Å^{-1} and $q = 1.55$ Å^{-1} in the out-of-plane scattering direction are from cellulose $(1\ \bar{1}\ 0)/(110)$ and cellulose (200) planes, respectively, whereas in-plane reflections are dominated by diffraction from cuticular waxes (Ye et al. 2020). Consistent with previous work, Fig. 1a shows diffraction from cellulose crystals in Col-0 hypocotyls preferentially in the out-of-plane direction, indicating a preferred cellulose crystal orientation along the thickness of the cell wall. In this work, we used GIWAXS to examine the effect of defects in biosynthesis of cell wall components on the organization of cellulose crystals, including their preferred orientation.

Cellulose deficient and pectin deficient Arabidopsis hypocotyls show loss of cellulose preferred orientation

To explore the connection between defects in the biosynthesis of cellulose, pectin, and xyloglucan and the nanoscale organization of cellulose in primary cell walls, we examined the preferred orientation of cellulose in 6-day-old dark grown (etiolated)

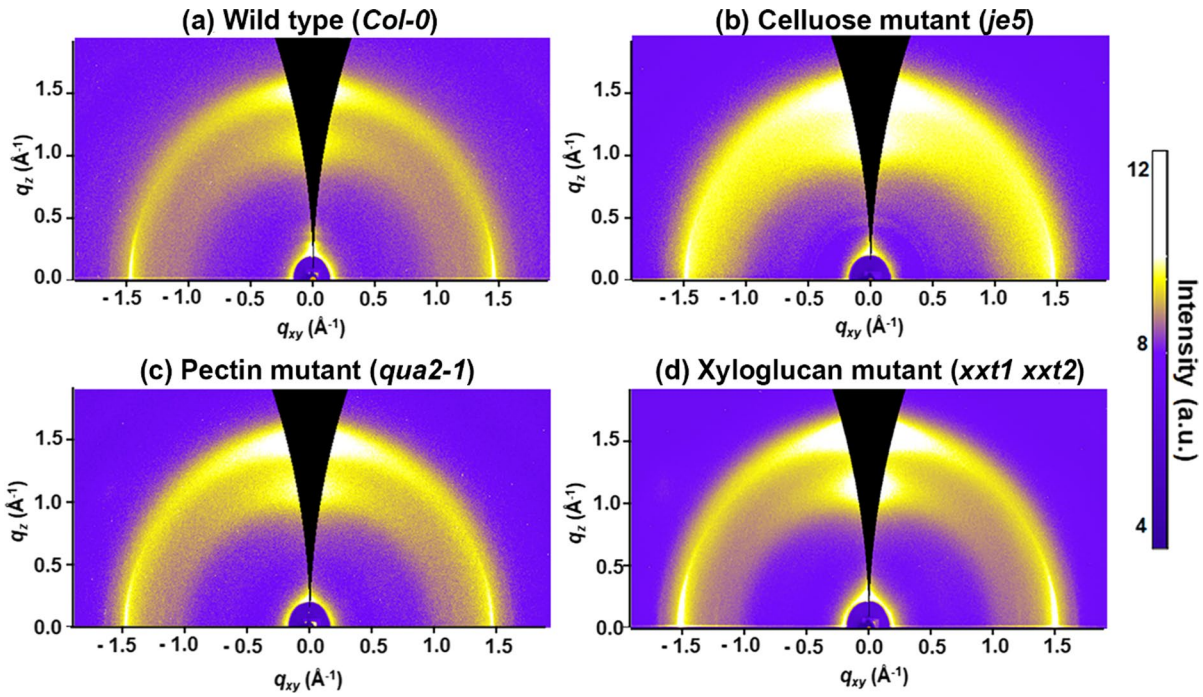

Fig. 1 GIWAXS 2D data from hypocotyls of dark grown 6-day-old *Arabidopsis thaliana* seedlings for **a** wild type *Columbia-0* (Col-0), **b** cellulose mutant *cesa3*^{je5} (*je5*), **c** pectin mutant *qua2-1*, and **d** xyloglucan mutant *xxt1 xxt2*. GIWAXS reveals a lower preferred orientation of cellulose crystals in cellulose and pectin deficient mutants when compared to the wild type, as shown by more isotropic scattering

hypocotyls of *Arabidopsis thaliana* mutants deficient in cellulose, pectin, or xyloglucan. Mutations in CESA isoforms, such as in *cesa3*^{je5} and *cesa6*$^{prc1-1}$, lead to reduced cellulose content and defects in cell elongation (Desnos et al. 1996; Fagard et al. 2000; Rui and Anderson 2016; Merz et al. 2017). Mutations not directly related to CESA can also affect cellulose crystallization, such as through loss of CSI1 in *csi1-3* null mutants that decouples CSC trajectories from microtubules. In addition, *jia1-1* is a missense mutation allele of KORRIGAN 1 that abolishes its endo-β-1,4 glucanase activity (Gu et al. 2010; Lei et al. 2014; Xin et al. 2020); cellulose deficiency also arises in these latter two mutants (*csi1-3* and *jia1-1*). *qua2-1* and *tsd2-1* are two mutant alleles of a pectin methyltransferase gene, *QUASIMODO2 (*QUA2), which is required for normal pectin synthesis (Frank et al. 2002; Mouille et al. 2003, 2007; Krupková et al. 2007; Bischoff et al. 2010; Du et al. 2020). These mutants exhibit reduced homogalacturonan (HG) content when compared to wild type, but show no significant change in the degree of methyl-esterification. The xyloglucan deficient *xxt1 xxt2* double mutant has defects in *XYLOGLUCAN XYLOSYLTRANSFERASE:* XXT1 and XXT2 genes (Cavalier et al. 2008), whereas *TmXXT2/xxt1 xxt2* complements the *xxt1 xxt2* double mutant with *TmXXT2* (*XXT2* from nasturtium, *Tropaeolum majus*) (Mansoori et al. 2015).

GIWAXS 2D images of 6-day-old dark grown hypocotyls of *cesa3*^{je5}, *qua2-1*, and *xxt1 xxt2* show two anisotropic reflections in the out-of-plane direction (meridional direction in Fig. 1) indicating that cellulose crystals have a preferred orientation, or texture, in these mutants. GIWAXS 2D images of cellulose deficient mutants *cesa6*$^{prc1-1}$, *csi1-3*, and *jia1-1*, pectin deficient mutant *tsd2-1*, and the *TmXXT2/xxt1 xxt2* complementation line also show preferred orientation of cellulose crystals (Fig. S2). Subtle changes, however, are observed in the reflections from cell wall mutants as compared to Col-0 wild type. Both reflections are more isotropic along the azimuthal (polar angle) direction in the mutants (Fig. S2). The angular spread of the reflections indicates loss of crystal

preferred orientation (Liman et al. 2013). Overall, more isotropic cellulose reflections are seen in the scattering patterns from cellulose deficient mutants and pectin deficient mutants when compared to wild type. Taken together, the GIWAXS 2D data indicate that the preferred orientation of cellulose crystals is likely disrupted in cellulose deficient mutants and pectin mutants, but not in xyloglucan deficient (or deficient and complemented) mutants, when compared to wild type.

Chain packing and cellulose crystal coherence length are altered in cellulose deficient mutants

Previous work shows perturbations to the chemical composition of the cell wall due to defects in the biosynthesis of cellulose (Fagard et al. 2000; Gu et al. 2010; Lei et al. 2014; Rui and Anderson 2016), pectin (Du et al. 2020), and xyloglucan (Cavalier et al. 2008). Changes in wall composition can potentially affect the nanoscale organization of cellulose; thus, we examined the effect of reduction of cell wall components on lattice spacings (glucan chain packing) and coherence length. We calculate out-of-plane and in-plane scattering profiles as shown in Figure S3, and the out-of-plane scattering profiles show subtle changes in the peak position of the scattering vector (q_z) in cell wall mutants when compared to scattering from wild type (Fig. 2a and Fig. S4a). As seen in Fig. 2a, the cellulose (200) reflection for wild type is found at q_z of 1.55 Å^{-1}. The cellulose (200) reflection shifts to a slightly lower q_z for the CSC-related cellulose mutants *cesa3*^{je5} and *cesa6*$^{prc1-1}$ (1.53 Å^{-1}), whereas the position of the (200) reflection does not change significantly for non-CSC related cellulose mutants *csi1-3* and *jia1-1,* pectin mutants *qua2-1* and *tsd2-1,* xyloglucan mutant *xxt1 xxt2*, and the *TmXXT2/xxt1 xxt2* complementation line when compared to values obtained from wild type (Figs. 2a and S4). The cellulose (1 $\bar{1}$ 0)/(110) reflection (q_z ~ 1.15 Å^{-1}) does not shift in the mutants in comparison to the wild type (Fig. 2a and Fig. S4a). In-plane 1D scattering profiles were also obtained from azimuthal integration of sectors over polar angles 78° to 88° of GIWAXS 2D data. The in-plane scattering profiles look similar for wild type and cell wall mutants, with only subtle changes in peak position. All Arabidopsis hypocotyls show a sharp peak at q_z ~ 1.51 Å^{-1} (Fig. S4b). This reflection is due to epicuticular wax crystals lining the outside of epidermal cell walls, as previously reported for GIWAXS data from primary cell walls (Ye et al. 2020).

Changes in the position of cellulose GIWAXS reflections can indicate changes in the spacings of

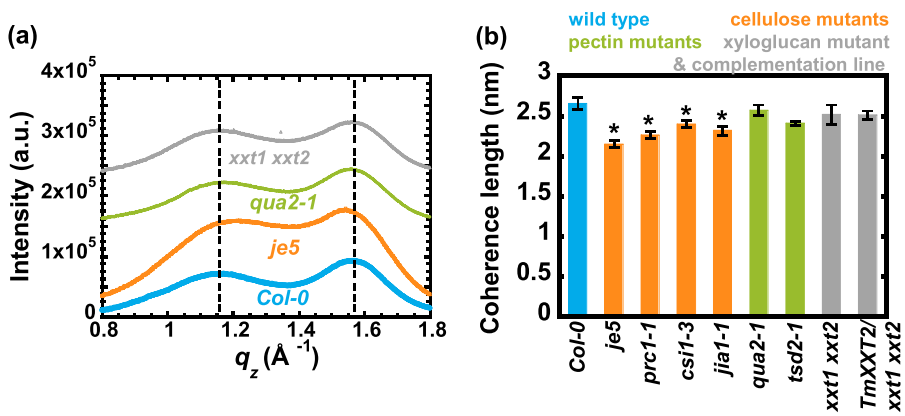

Fig. 2 GIWAXS data show that mutations affecting cellulose biosynthesis disrupt cellulose crystallization. **a** GIWAXS profiles of hypocotyls of dark grown 6-day-old *Columbia-0* wild type (Col-0; blue), cellulose mutant (*cesa3*^{je5} (*je5*); orange), pectin mutant (*qua2-1*; green), and xyloglucan mutant (*xxt1 xxt2*; gray) obtained from sector averages along the out-of-plane direction (q_z, sector average from − 17° to + 17°). Profiles are offset vertically for clarity. **b** Coherence lengths obtained from Scherrer's equation at the cellulose (200) reflection for wild type (Col-0; blue), cellulose mutants (*cesa3*^{je5} (*je5*), *cesa6*$^{prc1-1}$ (*prc1-1*), *csi1-3*, and *jia1-1*; orange), pectin mutants (*qua2-1* and *tsd2-1*; green), xyloglucan mutant (*xxt1 xxt2*; gray) and the complementation line (*TmXXT2/xxt1 xxt2*; gray). Error bars represent standard error of the mean and asterisks indicate statistically significant differences in comparison to the Col-0 wild type sample (*$p < 0.05$; n = 5 for Col-0, *qua2-1*, and *xxt1 xxt2*, n = 3 for *je5*, *prc1-1*, *csi1-3*, *jia1-1*, *tsd2-1*, and *TmXXT2/xxt1 xxt2*)

Table 1 d-spacings of cellulose (1 $\bar{1}$ 0)/(110) and cellulose (200) crystal planes calculated from q (scattering vector) positions of scattering peaks in out-of-plane profiles (d = 2π/q). Error bars represent standard error of the mean and asterisks indicate significant differences in comparison to the Col-0 wild type sample (*$p < 0.05$; sample sizes: n = 8 for Col-0, n = 5 for *qua2-1*, and *xxt1 xxt2*; n = 3 for *cesa3*^{je5} (*je5*), *cesa6*$^{prc1-1}$ (*prc1-1*), *csi1-3*, *jia1-1*, *tsd2-1*, and *TmXXT2/xxt1 xxt2*)

	d-spacing of Cellulose (1 $\bar{1}$ 0)/(110) (Å)	d-spacing of Cellulose (200) (Å)
Col-0	5.35 ± 0.02	4.06 ± 0.01
je5	5.33 ± 0.01	4.08 ± 0.01*
prc1-1	5.39 ± 0.02	4.08 ± 0.01*
csi1-3	5.31 ± 0.01	4.06 ± 0.01
jia1-1	5.29 ± 0.04	4.06 ± 0.01
qua2-1	5.39 ± 0.08	4.05 ± 0.01
tsd2-1	5.34 ± 0.02	4.06 ± 0.01
xxt1 xxt2	5.40 ± 0.05	4.06 ± 0.01
TmXXT2/xxt1 xxt2	5.36 ± 0.02	4.07 ± 0.01

cellulose (1 $\bar{1}$ 0)/(110) and cellulose (200) planes ($d = 2\pi/q_z$). As shown in Table 1, the d-spacings of cellulose (200) planes are significantly higher in *cesa3*^{je5} and *cesa6*$^{prc1-1}$ cellulose deficient mutants as compared to the Col-0 wild type, indicating a larger spacing between hydrogen-bonding planes of glucan sheets. The d-spacing of the cellulose (1 $\bar{1}$ 0)/(110) planes in cell wall mutants is not significantly different from that of wild type.

The coherence length, the distance over which the coherence between crystal planes is lost, has been used as an estimate of the average crystallite size of cellulose from cotton (*Gossypium hirsutum*), ramie (*Boehmeria nivea*), tunicates (subphylum *Tunicata*), *Acetobacter xylinum*, *Chaetomorpha melagonium* (Nieduszynski and Preston 1970), valonia (*Valonia ventricosa*) (Caulfield 1971), and spruce (*Picea spp.*) (Andersson et al. 2003). We used the FWHM of the cellulose (200) reflection to determine the coherence length of cellulose from Arabidopsis cell walls. The coherence lengths of cellulose mutants are significantly lower than that of the wild type (Fig. 2b and Table S1), whereas the coherence lengths of pectin and xyloglucan mutants are not significantly different from that of the wild type. Table S2 reports the 95% confidence intervals of differences of the means between the Col-0 wild type and the mutants examined. Smaller crystal coherence lengths in the cellulose deficient mutants than in the wild type suggests that mutations affecting cellulose biosynthesis disrupt the process by which glucan chains are assembled into partially crystalline cellulose microfibrils in the cell wall (Liu et al. 2016), leading to smaller or more defective crystals, such as through an increase in the degree of paracrystallinity (Rongpipi et al. 2019).

Preferred orientation of cellulose crystals is disrupted in cellulose mutants and pectin mutants but not in xyloglucan mutants

As shown in Fig. 1, the anisotropic cellulose reflections are indicative of a preferred orientation of cellulose crystals in primary cell walls, and the degree of anisotropy of cellulose reflections is reduced in cellulose deficient and pectin deficient mutants. We measure the changes in scattering through χ-pole figures that are constructed from a combination of GIWAXS data and rocking scans (Widjonarko et al. 2014; Ye et al. 2020). The widths of the χ-pole figures, which reflect the degree of anisotropy of the cellulose reflections, are a measure of the degree of preferred orientation of cellulose crystals. We compared the degree of preferred orientation or texture of cellulose crystals in wild type and cell wall mutants to elucidate how defects in the biosynthesis of cell wall components impact preferential alignment of cellulose crystal planes. We use the (1 $\bar{1}$ 0)/(110) reflection for χ-pole figures, because the Bragg reflection from epicuticular wax at $q_z \sim 1.51$ Å^{-1} in the in-plane scattering direction confounds χ-pole figures at the cellulose (200) reflection ($q \sim 1.55$ Å^{-1}) (Ye et al. 2020).

Figure 3a and Figure S5 show χ-pole figures obtained from the cellulose (1 $\bar{1}$ 0)/(110) reflection of Arabidopsis mutants and wild type. In Fig. 3a, the maximum intensity is normalized for all samples to highlight the change in breadth of the peak at a polar angle of zero. Some mutants, such as *je5*, show broader pole figures, indicating a loss of preferential alignment of cellulose crystals when compared to wild type. We can quantify the changes in preferred orientation with the width of the peak, where more narrow distributions and small peak widths indicate a higher degree of crystal texture. The widths of the χ-pole figures (Fig. 3a, Fig. S5, and Table S1) from the cellulose (1 $\bar{1}$ 0)/(110) reflection of Arabidopsis

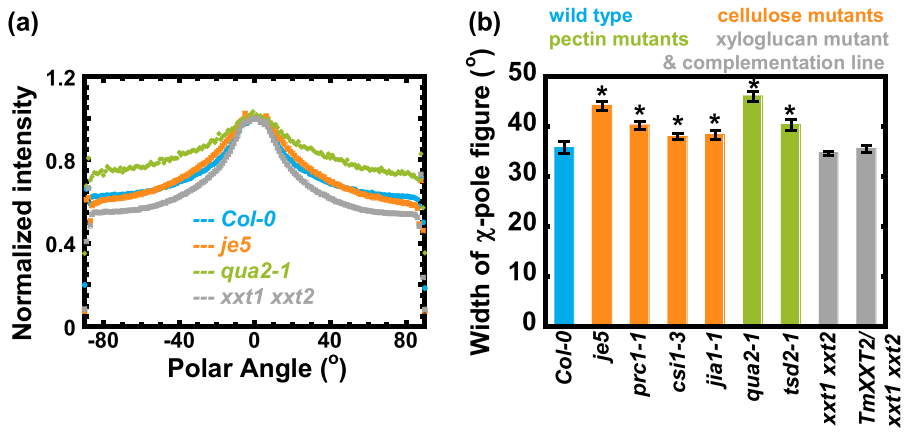

Fig. 3 Preferred cellulose crystal orientation is disrupted in cellulose and pectin mutants. **a** χ-pole figures from cellulose (1 $\bar{1}$ 0)/(110) reflections of wild type (Col-0; blue), cellulose deficient mutant (*cesa3*^{je5} (*je5*); orange), pectin deficient mutant (*qua2-1*; green), and xyloglucan deficient mutant (*xxt1 xxt2*; gray) normalized by the maximum intensity (polar angle = 0°). **b** Widths of χ-pole figures from the cellulose (1 $\bar{1}$ 0)/(110) reflections for wild type (Col-0; blue), cellulose mutants (*cesa3*^{je5} (*je5*), *cesa6*$^{prc1-1}$ (*prc1-1*), *csi1-3*, and *jia1-1*; orange), pectin mutants (*qua2-1* and *tsd2-1*; green), xyloglucan mutant (*xxt1 xxt2;* gray*),* and the complementation line (*TmXXT2/xxt1 xxt2*; gray). Error bars represent standard error of the mean and asterisks indicate significant differences in comparison to the Col-0 wild type sample (*$p < 0.05$; $n = 5$ for Col-0, *qua2-1*, and *xxt1 xxt2*, $n = 3$ for *je5*, *prc1-1*, *csi1-3*, *jia1-1*, *tsd2-1*, and *TmXXT2/xxt1 xxt2*)

mutants and wild type shows differences as significantly higher FWHM for cellulose mutants and pectin mutants when compared to wild type (Fig. 3b and Table S1). The widths of χ-pole figures of xyloglucan mutants are not significantly different when compared to the wild type (Fig. 3b and Table S1). The 95% confidence intervals of differences of means between wild type and the examined mutants are reported in Table S2. These data show that the preferred orientation of cellulose crystals is reduced in cellulose and pectin deficient mutants, but it is not different from wild type in the xyloglucan deficient/complemented mutant.

Relative crystalline cellulose content in Arabidopsis hypocotyls is reduced in mutants as compared to wild type

The cellulose crystallinity in lignocellulosic biomass is an important determinant of its reactivity and accessibility (Rongpipi et al. 2019). The relative crystalline cellulose content in cell wall mutants was investigated to elucidate whether defects in the biosynthesis of cell wall components impact the crystalline order of cellulose in primary cell walls. Given the challenges with measuring absolute crystallinity (Rivnay et al. 2012), we obtained the relative crystalline cellulose content, also called the relative degree of crystallinity (Rivnay et al. 2011), by integrating the intensity of χ-pole figures corrected by the sine of the polar angle (χ) from − 90° to 90°. We normalized by sample thickness; sample thickness was measured by stylus profilometry. Profilometry reveals that the cell wall mutant samples examined, except for *TmXXT2/xxt1 xxt2*, are thicker than the Col-0 wild type cell wall (Fig. S6). Figure S7 shows sin(χ) corrected pole figures of Arabidopsis hypocotyls obtained from the cellulose (1 $\bar{1}$ 0)/(110) reflection. The relative crystalline cellulose content is significantly reduced in cellulose deficient mutants, pectin deficient mutants, and xyloglucan deficient mutants when compared to the Col-0 wild type sample (Fig. 4 and Table S1).

In vitro studies involving bacterial cellulose and composite pellicles (Martínez-Sanz et al. 2015) and cell wall materials from onion, carrot, and apple (Lopez-Sanchez et al. 2020) have reported that xyloglucan and pectin potentially interfere with cellulose crystallization and assembly processes. Previous reports involving genetic mutations have also shown that cellulose content, determined by the Updegraff method (Updegraff 1969), is significantly reduced in cellulose mutants *cesa3*^{je5}, *cesa6*$^{prc1-1}$, *csi1-3*, and *jia1-1*, pectin mutants *qua2-1* and *tsd2-1*, and the xyloglucan mutant *xxt1 xxt2* when compared to wild

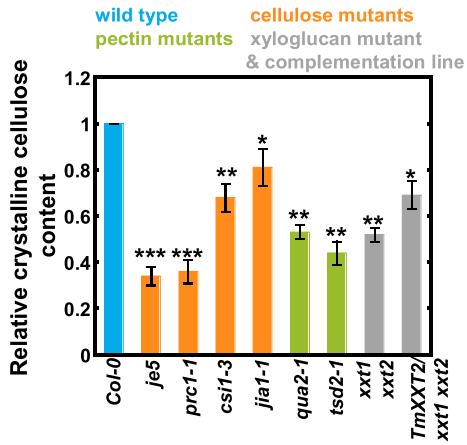

Fig. 4 Relative crystalline cellulose content of wild type (Col-0; blue), cellulose mutants (*cesa3*^{je5} (*je5*), *cesa6*$^{prc1-1}$ (*prc1-1*), *csi1-3*, and *jia1-1*; orange), pectin mutants (*qua2-1* and *tsd2-1*; green), xyloglucan mutant (*xxt1 xxt2;* gray*)* and the complementation line (*TmXXT2/xxt1 xxt2*; gray) determined from the integrated intensity of corrected χ-pole figures normalized by the sample thickness obtained from stylus profilometry. Data are normalized by the value for the wild type sample. Error bars represent standard error of the mean and asterisks indicate statistically significant differences in comparison to the Col-0 wild type sample (*$p<10^{-2}$, **$p<10^{-3}$, ***$p<10^{-5}$; n = 5 for Col-0, *qua2-1*, and *xxt1 xxt2*, n = 3 for *je5*, *prc1-1*, *csi1-3*, *jia1-1*, *tsd2-1*, and *TmXXT2/xxt1 xxt2*)

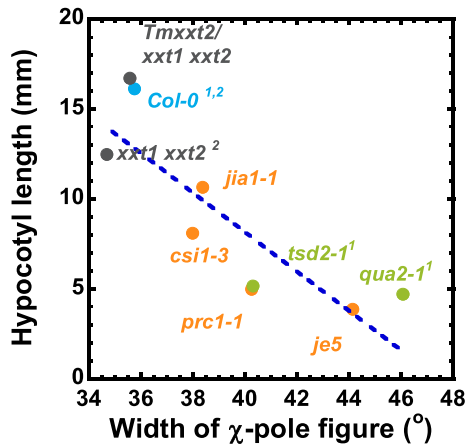

Fig. 5 Width of χ-pole figure at the cellulose (1 $\bar{1}$ 0)/(110) reflection versus hypocotyl length of 6-day-old dark grown Arabidopsis hypocotyls (wild type: Col-0 (blue); cellulose mutants: *cesa3*^{je5} (*je5*), *cesa6*$^{prc1-1}$ (*prc1-1*), *csi1-3*, and *jia1-1* (orange); pectin mutants: *qua2-1* and *tsd2-1* (green), xyloglucan mutant: *xxt1 xxt2* (gray), and the complementation line: *TmXXT2/xxt1 xxt2* (gray)). A linear fit to the data is shown as a dotted blue line. Pearson correlation analysis reveals a negative correlation (r = − 0.840, $p = 0.004$) and the 95% confidence interval of the slope (− 1.62, − 0.32) does not include zero. Superscripts denote sources for hypocotyl lengths: [1]Du et al., The Plant Cell (2020); [2]Xiao et al., Plant Physiology (2016). Hypocotyl lengths of Col-0, *je5, prc1-1, csi1-3*, *jia1-1,* and *TmXXT2* were measured in this study. The hypocotyl length of Col-0 used for the analysis is an average of the measurements obtained in the current study and in references [1]Du et al., The Plant Cell (2020) and.[2]Xiao et al., Plant Physiology (2016)

type (Fagard et al. 2000; Gu et al. 2010; Pysh et al. 2012; Lei et al. 2014; Rui and Anderson 2016; Xiao et al. 2016; Du et al. 2020). We find that the relative crystalline cellulose content obtained from χ-pole figures is positively correlated with the crystalline cellulose content obtained from the Updegraff method for 6-day-old etiolated hypocotyls of Col-0 wild type, *cesa3*^{je5}, *qua2-1*, *tsd2-1, xxt1 xxt2, and TmXXT2/xxt1 xxt2* mutants (Fig. S8). Reduced relative crystalline cellulose content in mutants with defects in cellulose biosynthesis is expected due to disruption in crystallization of cellulose, whereas reduced relative crystalline cellulose content in cell wall mutants deficient in matrix polysaccharides suggests that a reduction in the quantity of pectin and xyloglucan can perturb cellulose crystallization.

Degree of preferred orientation of cellulose crystals is correlated to hypocotyl length

We observe that Arabidopsis seedlings with a reduced degree of preferred orientation of cellulose from χ-pole figures have shorter hypocotyl lengths when compared to wild type. Previous work has hypothesized that cell elongation directly involves cellulose microfibril straightening, bending, sliding, and reorientation (Refrégier et al. 2004; Anderson et al. 2010; Zhang et al. 2021), which can potentially affect the preferred orientation of cellulose, i.e., crystal texturing. To determine whether the preferred orientation of cellulose and cell elongation are correlated, we plot the width of the χ-pole figure of the cellulose (1 $\bar{1}$ 0)/(110) reflection versus the hypocotyl length of different genotypes of *Arabidopsis thaliana*. An inverse linear relationship is observed between the width of the χ-pole figure and the hypocotyl length (Fig. 5), such that the hypocotyl length is positively correlated with the preferred orientation of cellulose crystals.

A gradient in cell length is found between the apical top region (near cotyledons) and the basal bottom

region (near roots) of dark grown Col-0 hypocotyls. Cell lengths measured using confocal microscopy show that the length of cells found in the bottom region (549 ± 185 μm) is significantly greater than that of cells located in the top region (247 ± 185 μm) of the hypocotyls. We find that the width of the χ-pole figure is significantly greater for the top region than for the bottom region, suggesting that the degree of preferred orientation of cellulose is higher in the bottom region than in the top region (Fig. S9a). Furthermore, the width of the χ-pole figures is correlated with the cell length within different regions of Col-0 hypocotyls (Fig. S9b).

Discussion

Cellulose microfibrils are synthesized by multimeric complexes of cellulose synthase proteins and extruded into the extracellular space during cell wall assembly in plants. Mutations in CESA genes or CSC-associated genes can disrupt cellulose deposition and organization in the cell wall. For example, *cesa3*^{je5} (Rui and Anderson 2016) and *cesa6*$^{prc1-1}$ (Fagard et al. 2000; MacKinnon et al. 2006) mutants have reduced crystalline cellulose content when compared to wild type, implying increased disorder in the arrangement of glucan chains within a cellulose microfibril. The organization of cellulose microfibrils in *cesa6*$^{prc1-1}$ has also been found to be altered when compared to wild type (MacKinnon et al. 2006; Park et al. 2019). It has been speculated that the altered cellulose organization could be a result of altered assembly, orientation, or function of the CSC. In fact, reduced CSC velocity has been reported in dark grown hypocotyls of *cesa6*$^{prc1-1}$ (Bischoff et al. 2011). Defects in the linkages between the CSC and cortical microtubules, a reduced velocity of CSCs in the plasma membrane when compared to the wild type, and disruption of the crossed-polylamellate architecture of the cell wall have been observed in *csi1-3* mutants (Li et al. 2012). In addition, perturbation of the organization of cortical microtubules and CSC trajectories have been observed in the *jia1-1* mutant, where cellulose crystallization is also disrupted (Lei et al. 2014). Overall, GIWAXS data are consistent with these previous findings and reveal that cellulose deficient mutants show decreased coherence lengths for the (200) reflection (Fig. 2), reduced cellulose crystallinity (Fig. 4), and a reduced preferred orientation of cellulose crystals along the thickness of the cell wall, i.e., a reduced cellulose texture (Fig. 3). The enhancement observed in microfibril co-alignment in *xxt1 xxt2* mutants through atomic force microscopy images (Xiao et al. 2016), however, does not correlate to a difference in crystal texture when compared to wild type (Fig. 3), highlighting the differences between these types of cellulose organization.

Here, we also show that the d-spacing for the cellulose (200) plane is larger in cellulose deficient CESA mutants, but not in cellulose deficient non-CESA mutants, when compared to wild type. Glucan chain packing in a cellulose microfibril potentially depends on how the CESA units are assembled by the CSC, and therefore, the incorporation of a defective CESA unit into a CSC could result in altered d-spacing. In the non-CESA cellulose mutants examined, however, the CESA units or their assembly in a CSC likely remain unaffected and thus the d-spacing remains unaltered in comparison to wild type.

Additionally, we observe that the coherence lengths of cellulose crystals are reduced in cellulose-related mutants but not in pectin and xyloglucan mutants, when compared to wild type. Cellulose crystal coherence lengths have been reported to be affected by the degree of crosslinks it has with other cell wall components (Liu et al. 2016). In the pectin and xyloglucan mutants, matrix components are also reduced concomitantly with reduction in cellulose, such that the degree of crosslinking may not be altered enough to affect the coherence length.

Previous measurements of cellulose content in cell wall mutants, as determined by fluorescence imaging techniques (leaves of light-treated *cesa3*^{je5}) (Rui and Anderson 2016), sum-frequency-generation (SFG) spectroscopy (dark grown hypocotyls of *qua2-1* and *tsd2-1*) (Du et al. 2020), and Fourier-transform infrared (FTIR) microspectroscopy (dark grown hypocotyls of *cesa6*$^{prc1-1}$) (Fagard et al. 2000), show a reduced cellulose content (Rui and Anderson 2016). Results shown in Fig. 4 are consistent with these findings and reveal that all mutants examined in this study exhibit a reduced crystalline cellulose content in comparison to the Col-0 wild type. Furthermore, the relative crystalline cellulose content obtained from pole figures for Col-0, *cesa3*^{je5}, *qua2-1*, *tsd2-1*, *xxt1 xxt2*, and *TmXXT2/xxt1 xxt2* correlates with crystalline

cellulose content obtained from the Updegraff method (Fig. S8). Reduced crystallinity in the xyloglucan deficient *xxt1 xxt2* mutant has been attributed to diminished cellulose synthase activity resulting from lower CSC particle density and lower speed in the plasma membrane (Xiao et al. 2016). Reduced crystallinity seen in pectin deficient mutants could be an effect of potentially decreased levels of demethyl-esterified HG. Low levels of demethyl-esterified HG have been found to correlate with high cellulose degradability, and thus low cellulose crystallinity, in Arabidopsis (Francocci et al. 2013). Although the degree of methyl esterification is not affected in these mutants, absolute levels of methyl esterified pectin are reduced with the reduction of total HG content (Daher and Braybrook 2015).

The *TmXXT2/xxt1 xxt2* complementation line has been shown to be functionally similar to wild type *Arabidopsis thaliana* (Mansoori et al. 2015). We have also found no significant difference between *TmXXT2/xxt1 xxt2* and Col-0 wild type with respect to hypocotyl length, cellulose preferred orientation, chain packing, and coherence length. It is, however, seen that the relative crystalline cellulose content is reduced in the complementation line when compared to wild type. This could potentially imply that complementing the *xxt1 xxt2* mutant with the *XXT2* gene from nasturtium does not fully restore the phenotype of crystalline cellulose content.

Pectin-related mutants, *qua2-1* and *tsd2-1*, exhibit a reduced cellulose preferred orientation, whereas the xyloglucan *xxt1 xxt2* mutant does not, even though both exhibit reduced cellulose crystalline content when compared to wild type. We highlight these consequences in schematics shown in Figure S10. Differences in interactions between pectin and xyloglucan with cellulose could lead to distinct consequences for cellulose texture. Previous models of primary cell walls assumed that xyloglucans coat the surface of cellulose microfibrils, and that they cross-link adjacent microfibrils or cross-link microfibrils and other matrix polysaccharides such as pectin (Cosgrove 2001; Somerville et al. 2004). There are several in vitro studies reporting non-covalent interactions between xyloglucan and cellulose microfibrils (Hayashi et al. 1987; Whitney et al. 1995; Pauly et al. 1999). Similarly, several in vitro studies report interactions between pectin and cellulose as well (Zykwinska et al. 2005, 2007; Broxterman and Schols 2018). 2D and 3D ^{13}C solid state NMR results of primary cell walls of *Arabidopsis thaliana* seem to contradict the xyloglucan-tether network model. They suggest that cellulose, hemicellulose, and pectins form a cohesive network in which all components are in molecular contact with each other (Dick-Pérez et al. 2011; Dick-Perez et al. 2012; Wang et al. 2012).

A study using biomechanical assays after enzymatic treatments of primary cell walls of cucumber hypocotyls has also contradicted the model of xyloglucan acting as tethers between cellulose microfibrils (Park and Cosgrove 2012). NMR of primary cell walls in *Arabidopsis thaliana* revealed cellulose-pectin contacts, potentially suggesting greater spatial proximity between pectin and cellulose than between xyloglucan and cellulose in primary cell walls (Dick-Pérez et al. 2011; Wang et al. 2012, 2015). Although we cannot identify the mechanism of how matrix polysaccharides affect cellulose microfibril organization and cellulose crystallization, our work is consistent with the hypothesis that cellulose potentially interacts extensively with pectin during wall assembly and is not simply coated/tethered by xyloglucan. Additionally, a previous study reported that pectin and xyloglucan compete with each other to bind with primary cell wall cellulose (Zykwinska et al. 2008). The study reported that pectin binds loosely to cellulose when xyloglucan is in a higher proportion in cell walls, but pectin-cellulose association gets stronger in xyloglucan-poor cell walls. It is possible that in pectin mutants where the xyloglucan proportion is higher, the weak pectin-cellulose association contributes to a reduced degree of cellulose preferred orientation when compared to wild type, whereas in the xyloglucan mutant the strong pectin-cellulose association prevents any disruption in cellulose preferred orientation. Alternatively, the formation of helical bundles, which has been observed in some pectin mutants (Saffer et al. 2023), would decrease the degree of texturing, because the helical structure would prevent the alignment of one specific crystallographic direction with respect to the plane of the cell wall.

We found that the width of χ-pole figures of 6-day-old Arabidopsis hypocotyls and the hypocotyl length are negatively correlated (Fig. 5). Because the width of the pole figure is inversely related to the degree of preferred orientation of crystals, the hypocotyl length is positively correlated with the degree of cellulose

texture in the hypocotyls. We verified that this is not due to changes in the hypocotyl geometry, by normalizing χ-pole figures by the width of hypocotyls (Fig. S6). The same trends are observed when accounting for these changes in hypocotyl geometry (Fig. S11). Growth of dark grown (etiolated) hypocotyls is controlled primarily by cell elongation and cell division does not contribute significantly to their growth process (Gendreau et al. 1997). This implies that hypocotyl elongation is proportional to cell elongation, which potentially leads to reorganization of cellulose in the cell wall (Refrégier et al. 2004; Bidhendi and Geitmann 2016).

A similar correlation between cell elongation and preferred orientation of cellulose is seen in the different regions of etiolated Col-0 hypocotyls, where a gradient of cell elongation exists between the apical top region and basal bottom region. The length of cells found in the bottom region is significantly greater than that of cells located in the top region. We find that the corresponding degree of preferred orientation of cellulose is also higher in the bottom region than in the top region (Fig. S9a and b).

A previous study proposed that rapid cell elongation involves extensive remodeling of the cell wall polymer network and requires cellulose deposition (Refrégier et al. 2004). Cell enlargement, size, and shape are controlled by reversible and irreversible wall deformations (Ortega 2010). The natural process of cell wall biosynthesis is hypothesized to involve the deposition of cellulose crystals aligned along the microfibril axis (Sugiyama et al. 1994). We hypothesize that this process also leads to a correlation in the orientation of cellulose crystals, and therefore the crystal texturing (*i.e.*, preferred orientation), observed in Figs. 1 and 3. A disruption of the microfibril alignment that occurs during biosynthesis potentially perturbs the cell elongation process and could thereby lead to growth defects in hypocotyls. As such, the degree of preferred orientation that we observe using GIWAXS could be affected by the tension cell walls experience during cell elongation. Our work suggests that the perturbation to pectin biosynthesis in *qua2-1* and *tsd2-1* mutants could affect the cellulose deposition process and therefore reduce the degree of preferred orientation of cellulose crystals, while also affecting cell elongation in dark grown hypocotyls.

It is also possible that disrupted preferred orientation of cellulose in cellulose and pectin mutants is a result of biological responses to cell wall defects. The wall composition and structure undergo active modification in response to specific functional requirements. One of the regulatory processes that maintains the functional integrity of cell walls is the cell wall integrity maintenance mechanism (Gigli-Bisceglia et al. 2020; Rui and Dinneny 2020). It monitors functional integrity of the cell wall and initiates compensatory responses to maintain the integrity. Genetic mutations affecting the biosynthesis of wall components induce growth defects in plants. For example, much shorter hypocotyls are seen in cellulose, pectin, and xyloglucan deficient mutants (Fagard et al. 2000; Xiao et al. 2016; Du et al. 2020) when compared to wild type. A previous report hypothesized that reduced cell elongation could be an effect of response to cell wall weakening that is caused by rapid cell elongation (Turner 2007). This weakening induces a cell wall stress that is similar to the weakening caused by degradation by pathogens. We expect that cellulose microfibrils in walls of cells with reduced elongation will experience reduced tensile force that can potentially lead to reduced cellulose preferred orientation in the dwarfed mutants. Although the xyloglucan mutant *xxt1 xxt2* also has shorter hypocotyls when compared to wild type, the difference in hypocotyl length between wild type and *xxt1 xxt2* is much smaller than in the case of the cellulose and pectin mutants studied here (Fagard et al. 2000; Lei et al. 2012; Lei et al. 2014; Xiao et al. 2016; Merz et al. 2017; Du et al. 2020). This smaller difference in cell elongation may not manifest as a significant reduction in cellulose preferred orientation. Additionally, a previous study reported that xyloglucan is not essential for the integrity of the cellulose network in the primary cell walls regenerated from Arabidopsis protoplasts (Kuki et al. 2020). Thus, xyloglucan deficiency may have lesser effects on the cell wall integrity as compared to cellulose or pectin deficiency. Furthermore, defective pectin biosynthesis in the cell wall has been reported to threaten cell wall integrity (Bethke et al. 2016; Du et al. 2020). Cell wall sensor genes have been found to be significantly downregulated in pectin deficient mutants *qua2-1* and *tsd2-1* (Du et al. 2020).

In summary, GIWAXS experiments of dark grown 6-day-old hypocotyls of wild type and mutant *Arabidopsis thaliana* demonstrate that defects in the biosynthesis of cell wall components affect the nanoscale organization of cellulose in primary cell walls. We

show that χ-pole figures constructed through a combination of GIWAXS and rocking scans reveal a type of cellulose organization, the cellulose preferred orientation with respect to the plant cell wall plane, and how this organization is disrupted in cellulose deficient and pectin deficient mutants, but not in xyloglucan deficient mutants of Arabidopsis. The invariance of cellulose organization in xyloglucan mutants could be a result of pectin-cellulose interactions impacting cellulose texture more than xyloglucan-cellulose interactions. We also found that the degree of preferred orientation of cellulose is correlated with hypocotyl elongation, suggesting a correlation with cell extension. Taken together, our results suggest that cell wall biosynthesis and assembly processes lead to a preferred orientation of cellulose crystals with respect to the plane of the cell wall, and that disruption of this organization might disrupt cell elongation and therefore plant growth.

Acknowledgments This work was supported as part of the Center for Lignocellulose Structure and Formation, an Energy Frontier Research Center funded by the US Department of Energy, Office of Science, Basic Energy Sciences under award no. DE-SC0001090. The authors acknowledge Beth Ann Jones and William John Mahoney III at the Materials Research Institute, The Pennsylvania State University for help with stylus profilometry measurements of Arabidopsis hypocotyls. The Advanced Light Source is supported by the Director, Office of Science, Office of Basic Energy Sciences, of the U.S. Department of Energy under Contract No. DE-AC02-05CH11231. This work is also based upon research conducted at the Stanford Synchrotron Radiation Lightsource, SLAC National Accelerator Laboratory, supported by the U.S. Department of Energy, Office of Science, Office of Basic Energy Sciences under Contract No. DE-AC02-76SF00515.

Author Contributions SR, EDG and EWG prepared figures and wrote the main manuscript text. WJB, OS, SD, XX, YG, and CAT grew plants and assisted with sample preparation and microscopy. SR, DY, JTDM, CZ, and MFT carried out X-ray experiments. All authors reviewed the manuscript.

Funding This work was supported by the Center for Lignocellulose Structure and Formation, an Energy Frontier Research Center funded by the US Department of Energy, Office of Science, Basic Energy Sciences under award no. DE-SC0001090. The Advanced Light Source is supported by the Director, Office of Science, Office of Basic Energy Sciences, of the U.S. Department of Energy under Contract No. DE-AC02-05CH11231. The Stanford Synchrotron Radiation Lightsource, SLAC National Accelerator Laboratory, is supported by the U.S. Department of Energy, Office of Science, Office of Basic Energy Sciences under Contract No. DE-AC02-76SF00515.

Data availability All raw data that supports the findings of this study are available from the corresponding authors (E.D.G, EW.G.) upon reasonable request.

Declarations

Conflict of interest The authors have no competing interests to disclose.

Ethical approval Not applicable, no animal or human studies.

References

Altman N, Krzywinski M (2017) P values and the search for significance. Nat Methods 14:3–4. https://doi.org/10.1038/nmeth.4120

Anderson CT, Carroll A, Akhmetova L, Somerville C (2010) Real-time imaging of cellulose reorientation during cell wall expansion in *Arabidopsis* roots. Plant Physiol 152:787–796. https://doi.org/10.1104/pp.109.150128

Andersson S, Serimaa R, Paakkari T, SaranpÄÄ P, Pesonen E (2003) Crystallinity of wood and the size of cellulose crystallites in Norway spruce (*Picea abies*). J Wood Sci 49:531–537. https://doi.org/10.1007/s10086-003-0518-x

Bethke G, Thao A, Xiong G, Li B, Soltis NE, Hatsugai N, Hillmer RA, Katagiri F, Kliebenstein DJ, Pauly M, Glazebrook J (2016) Pectin biosynthesis is critical for cell wall integrity and immunity in *Arabidopsis thaliana*. Plant Cell 28:537–556. https://doi.org/10.1105/tpc.15.00404

Bidhendi AJ, Geitmann A (2016) Relating the mechanics of the primary plant cell wall to morphogenesis. J Exp Bot 67:449–461. https://doi.org/10.1093/jxb/erv535

Bischoff V, Nita S, Neumetzler L, Schindelasch D, Urbain A, Eshed R, Persson S, Delmer D, Scheible W-R (2010) TRICHOME BIREFRINGENCE and its homolog AT5G01360 encode plant-specific DUF231 proteins required for cellulose biosynthesis in *Arabidopsis*. Plant Physiol 153:590–602. https://doi.org/10.1104/pp.110.153320

Bischoff V, Desprez T, Mouille G, Vernhettes S, Gonneau M, Höfte H (2011) Phytochrome regulation of cellulose synthesis in *Arabidopsis*. Curr Biol 21:1822–1827. https://doi.org/10.1016/j.cub.2011.09.026

Broxterman SE, Schols HA (2018) Interactions between pectin and cellulose in primary plant cell walls. Carbohydr Polym 192:263–272. https://doi.org/10.1016/j.carbpol.2018.03.070

Carpita NC, Gibeaut DM (1993) Structural models of primary cell walls in flowering plants: consistency of molecular structure with the physical properties of the walls during growth. Plant J 3:1–30. https://doi.org/10.1111/j.1365-313x.1993.tb00007.x

Caulfield DF (1971) Crystallite sizes in wet and dry *Valonia ventricosa*. Text Res J 41:264–280. https://doi.org/10.1177/004051757104100313

Cavalier DM, Lerouxel O, Neumetzler L, Yamauchi K, Reinecke A, Freshour G, Zabotina OA, Hahn MG, Burgert I, Pauly M, Raikhel NV, Keegstra K (2008) Disrupting Two *Arabidopsis thaliana* Xylosyltransferase genes results in plants deficient in Xyloglucan, a Major primary cell wall component. Plant Cell 20:1519–1537. https://doi.org/10.1105/tpc.108.059873

Cosgrove DJ (2001) Wall structure and wall loosening. a look backwards and forwards. Plant Physiol 125:131–134. https://doi.org/10.1104/pp.125.1.131

Cosgrove DJ (2005) Growth of the plant cell wall. Nat Rev Mol Cell Biol 6:850–861. https://doi.org/10.1038/nrm1746

Cutler SR, Ehrhardt DW, Griffitts JS, Somerville CR (2000) Random GFP::cDNA fusions enable visualization of subcellular structures in cells of Arabidopsis at a high frequency. Proc Natl Acad Sci USA 97:3718–3723. https://doi.org/10.1073/pnas.97.7.3718

Daher FB, Braybrook SA (2015) How to let go: pectin and plant cell adhesion. Front Plant Sci. https://doi.org/10.3389/fpls.2015.00523

Del Mundo JT, Rongpipi S, Yang H, Ye D, Kiemle SN, Moffitt SL, Troxel CL, Toney MF, Zhu C, Kubicki JD, Cosgrove DJ, Gomez EW, Gomez ED (2023) Grazing-incidence diffraction reveals cellulose and pectin organization in hydrated plant primary cell wall. Sci Rep 13:5421. https://doi.org/10.1038/s41598-023-32505-8

Desnos T, Orbovic V, Bellini C, Kronenberger J, Caboche M, Traas J, Hofte H (1996) Procuste1 mutants identify two distinct genetic pathways controlling hypocotyl cell elongation, respectively in dark- and light-grown *Arabidopsis* seedlings. Development 122:683–693. https://doi.org/10.1242/dev.122.2.683

Desprez T, Juraniec M, Crowell EF, Jouy H, Pochylova Z, Parcy F, Höfte H, Gonneau M, Vernhettes S (2007) Organization of cellulose synthase complexes involved in primary cell wall synthesis in *Arabidopsis thaliana*. Proc Natl Acad Sci USA 104:15572–15577. https://doi.org/10.1073/pnas.0706569104

Dick-Pérez M, Zhang Y, Hayes J, Salazar A, Zabotina OA, Hong M (2011) Structure and interactions of plant cell-wall polysaccharides by two- and three-dimensional magic-angle-spinning solid-state NMR. Biochem 50:989–1000. https://doi.org/10.1021/bi101795q

Dick-Perez M, Wang T, Salazar A, Zabotina OA, Hong M (2012) Multidimensional solid-state NMR studies of the structure and dynamics of pectic polysaccharides in uniformly 13C-labeled *Arabidopsis* primary cell walls. Magn Reson Chem 50:539–550. https://doi.org/10.1002/mrc.3836

Du J, Kirui A, Huang S, Wang L, Barnes WJ, Kiemle S, Zheng Y, Rui Y, Ruan M, Qi S, Kim SH, Wang T, Cosgrove DJ, Anderson CT, Xiao C (2020) Mutations in the pectin methyltransferase QUASIMODO2 influence cellulose biosynthesis and wall integrity in *Arabidopsis thaliana*. Plant Cell 32:3576–3597. https://doi.org/10.1105/tpc.20.00252

Fagard M, Desnos T, Desprez T, Goubet F, Refregier G, Mouille G, McCann M, Rayon C, Vernhettes S, Höfte H (2000) PROCUSTE1 encodes a cellulose synthase required for normal cell elongation specifically in roots and dark-grown hypocotyls of *Arabidopsis*. Plant Cell 12:2409–2424. https://doi.org/10.1105/tpc.12.12.2409

Francocci F, Bastianelli E, Lionetti V, Ferrari S, De Lorenzo G, Bellincampi D, Cervone F (2013) Analysis of pectin mutants and natural accessions of *Arabidopsis* highlights the impact of de-methyl-esterified homogalacturonan on tissue saccharification. Biotechnol Biofuels 6:163–163. https://doi.org/10.1186/1754-6834-6-163

Frank M, Guivarc'h A, Krupková E, Lorenz-Meyer I, Chriqui D, Schmülling T (2002) TUMOROUS SHOOT DEVELOPMENT (TSD) genes are required for co-ordinated plant shoot development. Plant J 29:73–85. https://doi.org/10.1046/j.1365-313x.2002.01197.x

Gendreau E, Traas J, Desnos T, Grandjean O, Caboche M, Höfte H (1997) Cellular basis of hypocotyl growth in *Arabidopsis thaliana*. Plant Physiol 114:295–305. https://doi.org/10.1104/pp.114.1.295

Gigli-Bisceglia N, Engelsdorf T, Hamann T (2020) Plant cell wall integrity maintenance in model plants and crop species-relevant cell wall components and underlying guiding principles. Cell Mol Life Sci 77:2049–2077. https://doi.org/10.1007/s00018-019-03388-8

Gu Y, Kaplinsky N, Bringmann M, Cobb A, Carroll A, Sampathkumar A, Baskin TI, Persson S, Somerville CR (2010) Identification of a cellulose synthase-associated protein required for cellulose biosynthesis. Proc Natl Acad Sci USA 107:12866–12871. https://doi.org/10.1073/pnas.1007092107

Harris DM, Corbin K, Wang T, Gutierrez R, Bertolo AL, Petti C, Smilgies D-M, Estevez JM, Bonetta D, Urbanowicz BR, Ehrhardt DW, Somerville CR, Rose JKC, Hong M, DeBolt S (2012) Cellulose microfibril crystallinity is reduced by mutating C-terminal transmembrane region residues CESA1^{A903V} and CESA3^{T942I} of cellulose synthase. Proc Natl Acad Sci USA 109:4098–4103. https://doi.org/10.1073/pnas.1200352109

Hayashi T, Marsden MPF, Delmer DP (1987) Pea Xyloglucan and cellulose. Plant Physiol 83:384–389. https://doi.org/10.1104/pp.83.2.384

Hexemer A, Müller-Buschbaum P (2015) Advanced grazing-incidence techniques for modern soft-matter materials analysis. IUCrJ 2:106–125. https://doi.org/10.1107/s2052252514024178

Hexemer A, Bras W, Glossinger J, Schaible E, Gann E, Kirian R, MacDowell A, Church M, Rude B, Padmore H (2010) A SAXS/WAXS/GISAXS beamline with multilayer monochromator. J Phys Conf Ser 247:012007. https://doi.org/10.1088/1742-6596/247/1/012007

Jimison LH (2011) Understanding microstructure and charge transport in semicrystalline polythiophenes. Dissertation, Stanford

Krupková E, Immerzeel P, Pauly M, Schmülling T (2007) The TUMOROUS SHOOT DEVELOPMENT2 gene of *Arabidopsis* encoding a putative methyltransferase is required for cell adhesion and co-ordinated plant development. Plant J 50:735–750. https://doi.org/10.1111/j.1365-313X.2007.03123.x

Kuki H, Yokoyama R, Kuroha T, Nishitani K (2020) Xyloglucan is not essential for the formation and integrity of the cellulose network in the primary cell wall

regenerated from *Arabidopsis* protoplasts. Plants 9:629. https://doi.org/10.3390/plants9050629

Lei L, Li S, Gu Y (2012) Cellulose synthase interactive protein 1 (CSI1) mediates the intimate relationship between cellulose microfibrils and cortical microtubules. Plant Signal Behav 7:714–718. https://doi.org/10.4161/psb.20338

Lei L et al (2014) The jiaoyao1 mutant is an allele of korrigan1 that abolishes endoglucanase activity and affects the organization of both cellulose microfibrils and microtubules in *Arabidopsis*. Plant Cell 26:2601–2616. https://doi.org/10.1105/tpc.114.126193

Lerouxel O, Cavalier DM, Liepman AH, Keegstra K (2006) Biosynthesis of plant cell wall polysaccharides—a complex process. Curr Opin Plant Biol 9:621–630. https://doi.org/10.1016/j.pbi.2006.09.009

Li S, Lei L, Somerville CR, Gu Y (2012) Cellulose synthase interactive protein 1 (CSI1) links microtubules and cellulose synthase complexes. Proc Natl Acad Sci USA 109:185–190. https://doi.org/10.1073/pnas.1118560109

Liman CD, Choi S, Breiby DW, Cochran JE, Toney MF, Kramer EJ, Chabinyc ML (2013) Two-dimensional GIWAXS reveals a transient crystal phase in solution-processed thermally converted tetrabenzoporphyrin. J Phys Chem B 117:14557–14567. https://doi.org/10.1021/jp408220e

Liu J, Kim JI, Cusumano JC, Chapple C, Venugopalan N, Fischetti RF, Makowski L (2016) The impact of alterations in lignin deposition on cellulose organization of the plant cell wall. Biotechnol Biofuels 9:126. https://doi.org/10.1186/s13068-016-0540-z

Lopez-Sanchez P, Martinez-Sanz M, Bonilla MR, Sonni F, Gilbert EP, Gidley MJ (2020) Nanostructure and poroviscoelasticity in cell wall materials from onion, carrot and apple: Roles of pectin. Food Hydrocoll 98:105253. https://doi.org/10.1016/j.foodhyd.2019.105253

MacKinnon IM, Šturcová A, Sugimoto-Shirasu K, His I, McCann MC, Jarvis MC (2006) Cell-wall structure and anisotropy in procuste, a cellulose synthase mutant of *Arabidopsis thaliana*. Planta 224:438–448. https://doi.org/10.1007/s00425-005-0208-6

Mannsfeld S (2010) wxdiff: diffraction image processing and data analysis software. https://code.google.com/archive/p/wxdiff/

Mansoori N, Schultink A, Schubert J, Pauly M (2015) Expression of heterologous xyloglucan xylosyltransferases in *Arabidopsis* to investigate their role in determining xyloglucan xylosylation substitution patterns. Planta 241:1145–1158. https://doi.org/10.1007/s00425-015-2243-2

Martínez-Sanz M, Lopez-Sanchez P, Gidley MJ, Gilbert EP (2015) Evidence for differential interaction mechanism of plant cell wall matrix polysaccharides in hierarchically-structured bacterial cellulose. Cellulose 22:1541–1563. https://doi.org/10.1007/s10570-015-0614-2

Merz D, Richter J, Gonneau M, Sanchez-Rodriguez C, Eder T, Sormani R, Martin M, Hématy K, Höfte H, Hauser M-T (2017) T-DNA alleles of the receptor kinase THESEUS1 with opposing effects on cell wall integrity signaling. J Exp Bot 68:4583–4593. https://doi.org/10.1093/jxb/erx263

Mouille G, Robin S, Lecomte M, Pagant S, Höfte H (2003) Classification and identification of *Arabidopsis* cell wall mutants using Fourier-Transform InfraRed (FT-IR) microspectroscopy. Plant J 35:393–404. https://doi.org/10.1046/j.1365-313X.2003.01807.x

Mouille G, Ralet M-C, Cavelier C, Eland C, Effroy D, Hématy K, McCartney L, Truong HN, Gaudon V, Thibault J-F, Marchant A, Höfte H (2007) Homogalacturonan synthesis in *Arabidopsis thaliana* requires a Golgi-localized protein with a putative methyltransferase domain. Plant J 50:605–614. https://doi.org/10.1111/j.1365-313X.2007.03086.x

Nieduszynski I, Preston RD (1970) Crystallite size in natural cellulose. Nature 225:273–274. https://doi.org/10.1038/225273a0

Ortega JKE (2010) Plant cell growth in tissue. Plant Physiol 154:1244–1253. https://doi.org/10.1104/pp.110.162644

Pandolfi RJ, Allan DB, Arenholz E, Barroso-Luque L, Campbell SI, Caswell TA, Blair A, De Carlo F, Fackler S, Fournier AP, Freychet G, Fukuto M, Da G, Jiang Z, Krishnan H, Kumar D, Kline RJ, Li R, Liman C, Marchesini S, Mehta A, N'Diaye AT, Parkinson DY, Parks H, Pellouchoud LA, Perciano T, Ren F, Sahoo S, Strzalka J, Sunday D, Tassone CJ, Ushizima D, Venkatakrishnan S, Yager KG, Zwart P, Sethian JA, Hexemer A (2018) Xicam: a versatile interface for data visualization and analysis. J Synchrotron Radiat 25:1261–1270. https://doi.org/10.1107/s1600577518005787

Park YB, Cosgrove DJ (2012) A revised architecture of primary cell walls based on biomechanical changes induced by substrate-specific endoglucanases. Plant Physiol 158:1933–1943. https://doi.org/10.1104/pp.111.192880

Park S, Song B, Shen W, Ding S-Y (2019) A mutation in the catalytic domain of cellulose synthase 6 halts its transport to the Golgi apparatus. J Exp Bot 70:6071–6083. https://doi.org/10.1093/jxb/erz369

Patterson AL (1939) The scherrer formula for X-ray particle size determination. Phys Rev 56:978–982. https://doi.org/10.1103/PhysRev.56.978

Pauly M, Albersheim P, Darvill A, York WS (1999) Molecular domains of the cellulose/xyloglucan network in the cell walls of higher plants. Plant J 20:629–639. https://doi.org/10.1046/j.1365-313x.1999.00630.x

Preston RD (1974) Physical biology of plant cell walls. Chapman and Hall, London

Pysh L, Alexander N, Swatzyna L, Harbert R (2012) Four alleles of AtCESA3 form an allelic series with respect to root phenotype in *Arabidopsis thaliana*. Physiol Plant 144:369–381. https://doi.org/10.1111/j.1399-3054.2012.01575.x

Refrégier G, Pelletier S, Jaillard D, Höfte H (2004) Interaction between wall deposition and cell elongation in dark-grown hypocotyl cells in *Arabidopsis*. Plant Physiol 135:959–968. https://doi.org/10.1104/pp.104.038711

Rivnay J, Noriega R, Kline RJ, Salleo A, Toney MF (2011) Quantitative analysis of lattice disorder and crystallite size in organic semiconductor thin films. Phys Rev B 84:045203. https://doi.org/10.1103/PhysRevB.84.045203

Rivnay J, Mannsfeld SCB, Miller CE, Salleo A, Toney MF (2012) Quantitative determination of organic semiconductor microstructure from the molecular to device scale.

Chem Rev 112:5488–5519. https://doi.org/10.1021/cr3001109

Rongpipi S, Ye D, Gomez ED, Gomez EW (2019) Progress and opportunities in the characterization of cellulose—an important regulator of cell wall growth and mechanics. Front Plant Sci 9:1894. https://doi.org/10.3389/fpls.2018.01894

Rueden CT, Schindelin J, Hiner MC, DeZonia BE, Walter AE, Arena ET, Eliceiri KW (2017) Image J2: ImageJ for the next generation of scientific image data. BMC Bioinform 18:529. https://doi.org/10.1186/s12859-017-1934-z

Rui Y, Anderson CT (2016) Functional analysis of cellulose and xyloglucan in the walls of stomatal guard cells of *Arabidopsis*. Plant Physiol 170:1398–1419. https://doi.org/10.1104/pp.15.01066

Rui Y, Dinneny JR (2020) A wall with integrity: surveillance and maintenance of the plant cell wall under stress. New Phytol 225:1428–1439. https://doi.org/10.1111/nph.16166

Saffer AM, Baskin TI, Verma A, Stanislas T, Oldenbourg R, Irish VF (2023) Cellulose assembles into helical bundles of uniform handedness in cell walls with abnormal pectin composition. Plant J 116:855–870. https://doi.org/10.1111/tpj.16414

Somerville C, Bauer S, Brininstool G, Facette M, Hamann T, Milne J, Osborne E, Paredez A, Persson S, Raab T, Vorwerk S, Youngs H (2004) Toward a systems approach to understanding plant cell walls. Science 306:2206–2211. https://doi.org/10.1126/science.1102765

Sugiyama J, Chanzy H, Revol JF (1994) On the polarity of cellulose in the cell wall of Valonia. Planta 193:260–265. https://doi.org/10.1007/BF00192539

Takahashi J, Rudsander UJ, Hedenström M, Banasiak A, Harholt J, Amelot N, Immerzeel P, Ryden P, Endo S, Ibatullin FM, Brumer H, del Campillo E, Master ER, Vibe Scheller H, Sundberg B, Teeri TT, Mellerowicz EJ (2009) KORRIGAN1 and its aspen homolog PttCel9A1 decrease cellulose crystallinity in *Arabidopsis* stems. Plant Cell Physiol 50:1099–1115. https://doi.org/10.1093/pcp/pcp062

Taylor NG (2008) Cellulose biosynthesis and deposition in higher plants. New Phytol 178:239–252. https://doi.org/10.1111/j.1469-8137.2008.02385.x

Turner SR (2007) Cell walls: monitoring integrity with the kinase. Curr Biol 17:R541–R542. https://doi.org/10.1016/j.cub.2007.05.033

Turner S, Kumar M (2018) Cellulose synthase complex organization and cellulose microfibril structure. Philos Trans A Math Phys Eng Sci 376:20170048. https://doi.org/10.1098/rsta.2017.0048

Updegraff DM (1969) Semimicro determination of cellulose in biological materials. Anal Biochem 32:420–424. https://doi.org/10.1016/S0003-2697(69)80009-6

Wang T, Zabotina O, Hong M (2012) Pectin-cellulose interactions in the *Arabidopsis* primary cell wall from two-dimensional magic-angle-spinning solid-state nuclear magnetic resonance. Biochem 51:9846–9856. https://doi.org/10.1021/bi3015532

Wang T, Park YB, Cosgrove DJ, Hong M (2015) Cellulose-pectin spatial contacts are inherent to never-dried *Arabidopsis* primary cell walls: evidence from solid-state nuclear magnetic resonance. Plant Physiol 168:871–884. https://doi.org/10.1104/pp.15.00665

Whitney SEC, Brigham JE, Darke AH, Reid JSG, Gidley MJ (1995) In vitro assembly of cellulose/xyloglucan networks: ultrastructural and molecular aspects. Plant J 8:491–504. https://doi.org/10.1046/j.1365-313x.1995.8040491.x

Widjonarko NE, Schulz P, Parilla PA, Perkins CL, Ndione PF, Sigdel AK, Olson DC, Ginley DS, Kahn A, Toney MF, Berry JJ (2014) Impact of hole transport layer surface properties on the morphology of a polymer-fullerene bulk heterojunction. Adv Energy Mater 4:1301879. https://doi.org/10.1002/aenm.201301879

Xiao C, Zhang T, Zheng Y, Cosgrove DJ, Anderson CT (2016) Xyloglucan deficiency disrupts microtubule stability and cellulose biosynthesis in *Arabidopsis*, altering cell growth and morphogenesis. Plant Physiol 170:234–249. https://doi.org/10.1104/pp.15.01395

Xin X, Lei L, Zheng Y, Zhang T, Pingali SV, O'Neill H, Cosgrove DJ, Li S, Gu Y (2020) Cellulose synthase interactive1- and microtubule-dependent cell wall architecture is required for acid growth in Arabidopsis hypocotyls. J Exp Bot 71:2982–2994. https://doi.org/10.1093/jxb/eraa063

Ye D, Rongpipi S, Kiemle SN, Barnes WJ, Chaves AM, Zhu C, Norman VA, Liebman-Peláez A, Hexemer A, Toney MF, Roberts AW, Anderson CT, Cosgrove DJ, Gomez EW, Gomez ED (2020) Preferred crystallographic orientation of cellulose in plant primary cell walls. Nat Commun 11:4720. https://doi.org/10.1038/s41467-020-18449-x

Yu L, Yoshimi Y, Cresswell R, Wightman R, Lyczakowski JJ, Wilson LFL, Ishida K, Stott K, Yu X, Charalambous S, Wurman-Rodrich J, Terrett OM, Brown SP, Dupree R, Temple H, Krogh KBRM, Dupree P (2022) Eudicot primary cell wall glucomannan is related in synthesis, structure, and function to xyloglucan. Plant Cell 34:4600–4622. https://doi.org/10.1093/plcell/koac238

Zeng Y, Himmel ME, Ding S-Y (2017) Visualizing chemical functionality in plant cell walls. Biotechnol Biofuels 10:263. https://doi.org/10.1186/s13068-017-0953-3

Zhang W, Bombile JH, Weisen AR, Xie R, Colby RH, Janik MJ, Milner ST, Gomez ED (2019) Thermal fluctuations lead to cumulative disorder and enhance charge transport in conjugated polymers. Macromol Rapid Commun 40:1900134. https://doi.org/10.1002/marc.201900134

Zhang Y, Yu J, Wang X, Durachko DM, Zhang S, Cosgrove DJ (2021) Molecular insights into the complex mechanics of plant epidermal cell walls. Science 372:706–711. https://doi.org/10.1126/science.abf2824

Zykwinska AW, Ralet M-CJ, Garnier CD, Thibault J-FJ (2005) Evidence for in vitro binding of pectin side chains to cellulose. Plant Physiol 139:397–407. https://doi.org/10.1104/pp.105.065912

Zykwinska A, Gaillard C, Buléon A, Pontoire B, Garnier C, Thibault J-F, Ralet M-C (2007) Assessment of In vitro binding of isolated pectic domains to cellulose by adsorption isotherms, electron microscopy, and X-ray diffraction methods. Biomacromol 8:223–232. https://doi.org/10.1021/bm060292h

Zykwinska A, Thibault J-F, Ralet M-C (2008) Competitive binding of pectin and xyloglucan with primary cell wall cellulose. Carbohydr Polym 74:957–961. https://doi.org/10.1016/j.carbpol.2008.05.004